THE JOURNAL OF PHYSICAL CHEMISTRY B

Article

pubs.acs.org/JPCB

Electron Configuration and Hydrogen-Bonding Pattern in Several Thymine and Uracil Analogues Studied by $^{1}H-^{14}N$ NQDR and DFT/QTAIM

Janez Seliger,[†,‡,§] Veselko Žagar,[†] Magdalena Latosińska,[⊥] and Jolanta Natalia Latosińska[⊥]

[†]Jozef Stefan Institute, Jamova 39, 1000 Ljubljana, Slovenia

[‡]Faculty of Mathematics and Physics, University of Ljubljana, Jadranska 19, 1000 Ljubljana, Slovenia

[§]EN-FIST Centre of Excellence, Dunajska 156, 1000 Ljubljana, Slovenia

[⊥]Faculty of Physics, Adam Mickiewicz University, Umultowska 85, 61-614 Poznań, Poland

ABSTRACT: Some thio- and aza-derivatives of natural nucleobases uracil and thymine: 2-thiouracil, 4-thiouracil, 6-methyl-2-thiouracil, 6-azauracil, and 6-aza-2-thiothymine have been studied experimentally in solid state by $^{1}H-^{14}N$ NMR-NQR double resonance (NQDR) and theoretically by the Density Functional Theory (DFT)/Quantum Theory of Atoms in Molecules (QTAIM). The ^{14}N resonance frequencies have been measured at 173 and 295 K and assigned to particular nitrogen sites (—N═ and —NH—). The temperature factor has been found negligible. The changes in the molecular skeletons, electric charge distribution, intermolecular interactions pattern, and molecular aggregations caused by oxygen replacement with sulfur and carbon replacement with nitrogen are discussed in detail. Correlations between all the principal components of the ^{14}N quadrupole coupling tensor have been found helpful in the search for the experimental ^{14}N NQR frequencies, their assignment to a particular nitrogen positions and estimation of the strength of the inter- and intramolecular interactions. The variation in the NQR parameters have been mainly related to the variation in the population of π-electron orbital. For thiouracil derivatives a general trend is that the stronger the hydrogen bond is, the lower is the asymmetry parameter, while for thymine and 6-aza-2-thiotymine, the opposite relation holds. Differences in correlations of the principal components of the ^{14}N quadrupole coupling tensor at the amino and iminonitrogen positions in heterocyclic rings are discussed. The effect of C→H and C→N substitution at the amino nitrogen position and C→N substitution at the iminonitrogen position on the quadrupole coupling tensor is analyzed. This study also demonstrates the advantages of combining NQR and DFT/QTAIM to predict an unsolved crystalline structure of 4-thiouracil.

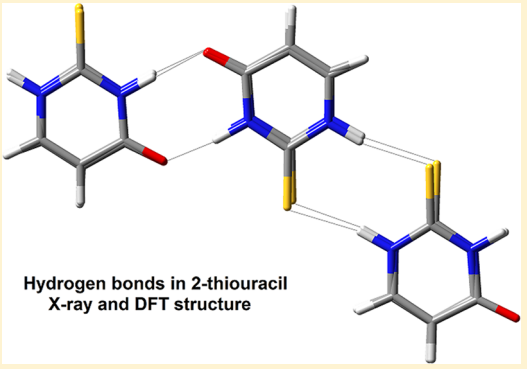

INTRODUCTION

The pyrimidine nucleobases of interest, uracil and thymine, belong to the building blocks of RNA and DNA, respectively. Both nucleobases bind with adenine via the N−H···O and N−H···N hydrogen bonds. It is known that the hydrophobic methyl group in thymine changes the chemical properties of uracil and restricts its pairing to adenine which greatly improves the efficiency of DNA replication, makes the repair mechanism more effective, and protects DNA against viruses or certain bacteria making it unrecognizable to many nucleases. In general, the hydrogen-bonds pattern is responsible not only for the secondary but also tertiary structure of DNA and RNA. Thus, clarification of the hydrogen-bonding mechanism is important to understand the base pairing as well as diverse functions ranging from molecular recognition to catalysis. Any alteration or modification in the base pairing scheme of DNA may result in its reduced stability. This feature has directed significant attention to those derivatives of uracil and thymine which may efficiently bind with DNA and thus can be used for intentional perturbation of the base-pairing scheme, including that leading to cessation of cell division.[1] Indeed, thio- or aza-substitution (i.e., replacement of oxygen by sulfur or carbon by nitrogen, respectively) in uracil or thymine changes the chemical properties and biological activity and leads to bioisosteric isomers possessing anticancer, antiviral, and antithyroid activities.[2−6] In some cases, high toxicity eliminates potent antitumor agents, for example, 6-azauracil, from clinical use.[7] Significant changes in the electron configuration properties of thio- and aza-nucleobases when compared to those of the natural ones are revealed not only in the chemical properties but also in the excited-state dynamics[8] which is directly related to their binding properties. In contrast to the natural bases, thio-nucleobases can be selectively photo-activated into the electronic triplet state with high affinity for cross-linking to other nucleic-acid bases and amino-acid residues.[9] Thus thio-derivatives have been used as intrinsic

Received: March 20, 2012
Revised: May 22, 2012
Published: July 2, 2012

dx.doi.org/10.1021/jp302659k | J. Phys. Chem. B 2012, 116, 8793−8804

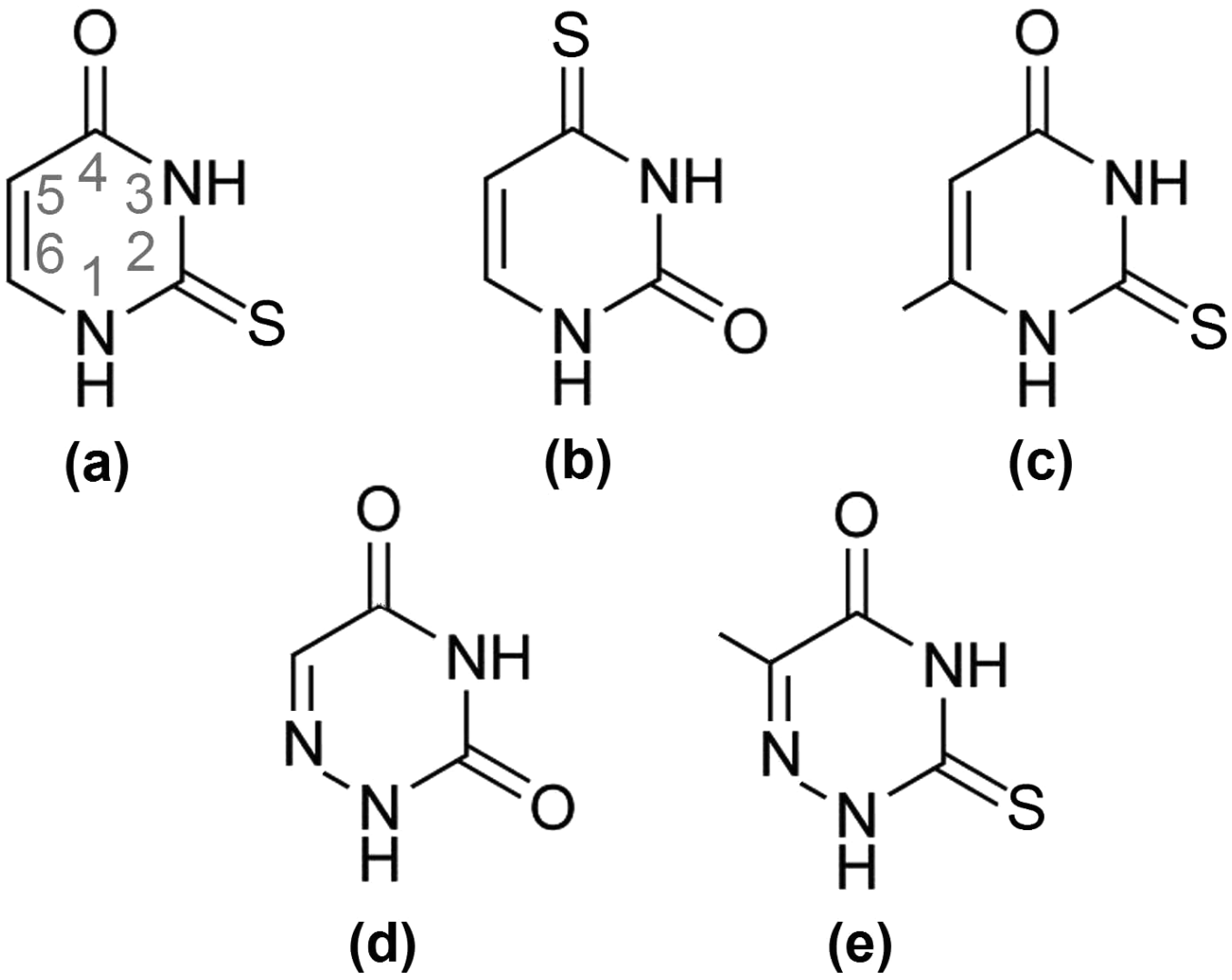

Figure 1. Structural formulas of 2-thiouracil (a), 4-thiouracil (b), 6-methyl-2 thiouracil (c), 6-azauracil (d), and 6-aza-2-thiothymine (e) and the numbering of positions.

photolabels to probe the structure and organization of RNA,[10,11] to identify the interactions between nucleic acids and proteins in nucleoprotein complexes,[12,13] and to follow the migration of electrons/holes in nucleic acids.[14]

In general the thio- or aza-nucleobases show a variety of chemical/physical/biological properties and applications, which is a consequence of modifications of electron density distribution and bonding capabilities in comparison to those of the natural nucleobases. In view of the above, it is of interest to investigate in detail the effect of nucleobases substitution by atoms definitely differing in electronegativity on the electron configuration and bonding pattern. For such a purpose a very sensitive tool which would allow investigation of details of the molecular and crystal structure, particularly sensitive to weak and short-range interactions, is required. A great potential of nuclear quadrupole resonance (NQR), molecular specific solid-state spectroscopy, offering a unique possibility of non-destructive characterization of molecular systems including biologically active ones in this application has been recently recognized.[22−25] NQR probes the electron configuration at specific atomic positions occupied by atoms possessing nuclear electric quadrupole moments. The electron configuration can be as well studied indirectly via the anisotropic chemical shift measured by NMR. The main advantage of using NQR is its high resolution, much higher in comparison to those of NMR. Thus as an experimental method for studies of uracil and thymine derivatives we have chosen ^{14}N NQR. The ^{14}N NQR frequencies that depend mainly on the electron configuration and to a lower degree on the bonding pattern are usually of several MHz and can be determined with an accuracy of several kHz or better.

In our previous papers we have shown that theoretical density functional theory (DFT), which reveals the global electron distribution density in the molecule is helpful for interpretation of complicated NQR spectra. The advantages of using a combination of NQR spectroscopy and DFT/quantum theory of atoms in molecule (QTAIM) approach for analysis of changes in the molecular skeletons, charge distribution, intermolecular interactions pattern, and molecular aggregations caused by oxygen replacement with sulfur have been discussed for 2-thiocytosine[15] and 6-thiouguanine,[16] potential and currently used antileukemia agents, respectively. In the present study we extended our investigation to 2-thiouracil, 4-thiouracil, 6-methyl-2-thiouracil, 6-azauracil, and 6-aza-2-thiothymine, Figure 1. The results of the present study are confronted

dx.doi.org/10.1021/jp302659k | J. Phys. Chem. B 2012, 116, 8793−8804

with those of the previous ^{14}N NQR studies of structurally related compounds.[15−25]

Although, at the moment there is only a limited number of experimental and theoretical NQR studies of biologically active molecules related to binding specificity, drug efficacy, toxicity, etc., we believe that a large number of these studies, together with related spectroscopic methods as for example NMR (nuclear magnetic resonance) and EPR (electron paramagnetic resonance), will help find correlations between chemical structure and biological properties. Some results of such a multispectroscopic joint studies have been already reported.[25] This study also demonstrates the advantages of combining NQR and DFT/QTAIM to predict an unsolved crystalline structure of 4-thiouracil. We hope that our systematic studies will contribute to the explanation of implications of substitution on the intermolecular bonding formation required for effective processes of recognition and binding to the proteins or DNA.

EXPERIMENTAL SECTION

The samples of 2-thiouracil, 4-thiouracil, 6-methyl-2-thiouracil, 6-azauracil and 6-aza-2-thiothymine have been purchased from Sigma-Aldrich and used as obtained.

(i). NQR. The electron configuration of a molecule can be studied indirectly by measuring the electric quadrupole interaction of atomic nuclei with the local electric field produced by the electron distribution. The Hamiltonian of a quadrupole atomic nucleus in the inhomogeneous local electric field and in zero external magnetic field reads[26]

$$H_Q = \frac{e^2qQ}{4I(2I-1)}\left(3I_z^{\,2} - I(I+1) + \frac{\eta}{2}(I_+^{\,2} + I_-^{\,2})\right) \quad (1)$$

Here eQ is the nuclear electric quadrupole moment, I is the nuclear spin and eq and η are the largest principal value and the asymmetry parameter of electric field gradient (EFG) tensor, respectively. The second rank traceless EFG tensor is composed of the second derivatives of the electrostatic potential with respect to the coordinates, taken at the position of the nucleus. The principal values of the EFG tensor are labeled as V_{ZZ}, V_{YY}, and V_{XX} ($|V_{ZZ}| \geq |V_{YY}| \geq |V_{XX}|$). The largest principal value $V_{ZZ} = eq$ measures the strength of the nuclear quadrupole interaction. The asymmetry parameter η is defined as $\eta = (V_{XX} - V_{YY})/V_{ZZ}$. It ranges between 0 and 1. In zero external electric field a quadrupole nucleus occupies either $(2I + 1)$ nondegenerate or $(2I + 1)/2$ doubly degenerate nuclear quadrupole energy levels depending on whether the nuclear spin is an integer or a half-integer, respectively. Two parameters, the quadrupole coupling constant e^2qQ/h, where h is the Planck constant, and the asymmetry parameter η, can be determined from the transition frequencies between the nuclear quadrupole energy levels, which are called the nuclear quadrupole resonance (NQR) frequencies. The principal values of the nuclear quadrupole coupling tensor q_{ii}, defined as $q_{ii} = eQV_{ii}/h$ ($I = X, Y, Z$), are calculated from e^2qQ/h and η as

$$q_{ZZ} = \frac{e^2qQ}{h}$$

$$q_{YY} = -\frac{e^2qQ}{2h}(1+\eta) = -\frac{q_{ZZ}}{2}(1+\eta)$$

$$q_{XX} = -\frac{e^2qQ}{2h}(1-\eta) = -\frac{q_{ZZ}}{2}(1-\eta) \quad (2)$$

In the present study we measured the NQR frequencies of the nitrogen nucleus ^{14}N. In the compounds studied, the nitrogen atom acts as a hydrogen-bond donor (−NH−) or as a hydrogen-bond acceptor (=N—). The ^{14}N NQR is thus sensitive to the electron charge distribution in the hydrogen bonds.

The nucleus ^{14}N has a spin $I = 1$. It thus can occupy in zero external magnetic field three generally nonequidistant and nondegenerate nuclear quadrupole energy levels and three NQR frequencies that are related to e^2qQ/h and η as

$$\nu_+ = \left|\frac{e^2qQ}{4h}\right|(3+\eta)$$

$$\nu_- = \left|\frac{e^2qQ}{4h}\right|(3-\eta)$$

$$\nu_0 = \nu_+ - \nu_- = \left|\frac{e^2qQ}{2h}\right|\eta \quad (3)$$

The quadrupole coupling constant and η are obtained from the ^{14}N NQR frequencies as

$$\frac{e^2qQ}{h} = \pm\frac{2}{3}(\nu_+ + \nu_-)$$

$$\eta = \frac{3(\nu_+ - \nu_-)}{\nu_+ + \nu_-} \quad (4)$$

The sign of the quadrupole coupling constant cannot be determined by NQR, thus only the absolute values are often listed.

(ii). Double Resonance. The ^{14}N NQR frequencies were measured by ^{1}H−^{14}N nuclear quadrupole double resonance (NQDR) based on magnetic field cycling.[27] NQDR is an indirect technique for detection of ^{14}N NQR frequencies via the influence of the ^{14}N nuclei on the proton NMR signal. A NQDR experiment is schematically presented in Figure 2. The sample, which must contain both protons and ^{14}N, is shuttled between two magnets. The proton spin system is first

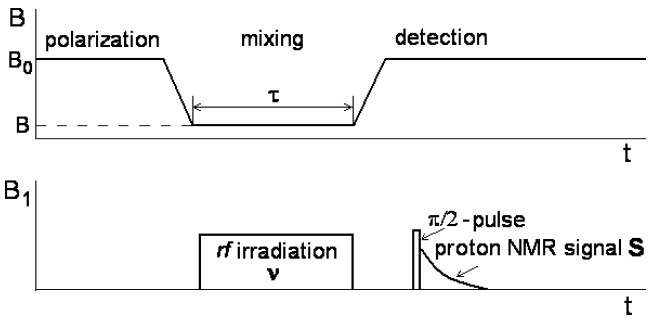

Figure 2. Schematic presentation of a NQDR cycle.

dx.doi.org/10.1021/jp302659k | J. Phys. Chem. B 2012, 116, 8793−8804

magnetized in a high magnetic field B_0, where it reaches the equilibrium magnetization M_0. The sample is then in a short time t, $t \approx 0.1$ s, transferred to a second magnet, where the magnetic field B is much lower than B_0. During the transfer the population of the proton Zeeman energy levels remains constant, whereas their splitting is reduced by the factor B/B_0. When the sample stops in the second magnet, the magnetization of the proton spin system is by the factor B_0/B greater than the equilibrium proton magnetization in the low-magnetic field B. The sample is left in the low magnetic field for a time τ, which is called the relaxation period. The proton magnetization relaxes during the relaxation period toward its equilibrium value in the low-magnetic field B and at the end of the relaxation period it reaches the value M,

$$\mathbf{M} = \frac{\mathbf{B}}{\mathbf{B}_0}\mathbf{M}_0 + \left(\mathbf{M}_0 - \frac{\mathbf{B}}{\mathbf{B}_0}\mathbf{M}_0\right)\exp(-\tau/T_1(\mathbf{B})) \quad (5)$$

Here $T_1(B)$ is the proton spin−lattice relaxation time in the low-magnetic field B. After the relaxation period, the sample is transferred back into the high magnetic field B_0 and the proton NMR is measured immediately after the sample stops in the high-magnetic field. The intensity of the proton NMR signal is proportional to the proton magnetization M. The proton NMR signal decreases with increasing τ according to eq 5, which is used to measure proton T_1 in the low-magnetic field B. A further decrease in the proton NMR signal at the end of the magnetic field cycle is obtained by double resonance.

In the level crossing[28,29] and solid-effect[30] techniques during the relaxation period a strong rf magnetic field with the frequency ν is applied. A decrease in the proton NMR signal is observed when ν is equal to the ^{14}N NQR frequency ν_Q (level crossing) and when ν is equal to $\nu_Q \pm \nu_H$ (solid effect). Here $\nu_H = \gamma_H B/(2\pi)$ is the proton Larmor frequency in the low magnetic field B. After a scan with the frequency ν, the ν-dependence of the proton NMR signal shows that the level crossing reaches the minima (dips) at $\nu = \nu_Q$ (Q = +, −, 0) and the solid effect at $\nu = \nu_Q \pm \nu_H$.

In the NQDR technique with the multiple frequency sweeps of an rf magnetic field and two-frequency irradiation,[31,32] at first the multiple frequency sweeps of rf magnetic field are applied during the relaxation period. The sweep range is chosen so that it covers the higher ^{14}N NQR frequencies ν_+ and ν_- . Always when during the sweep the frequency of the rf magnetic field reaches the ^{14}N NQR frequency ν_Q (Q = +, −), the population of the two ^{14}N nuclear quadrupole energy levels, separated in frequency by ν_Q, changes.

A scan is performed by the low magnetic field B in steps of 0.25 mT. When the proton Larmor frequency ν_H in the low magnetic field B matches the lowest ^{14}N NQR frequency ν_0, the multiple frequency sweeps produce a relaxation of the proton magnetization toward zero which is observed as a decrease in the proton NMR signal at the end of the magnetic field cycle. In the ν_H-dependence of the proton NMR signal, a dip is observed at $\nu_H = \gamma_H B/(2\pi) = \nu_0$.

In the second step of the experiment, the low magnetic field B is fixed at this dip and the scan is performed by one of the frequency limits (say the upper limit) of the frequency sweeps. When the upper frequency limit becomes lower than ν_+, the frequency sweeps cover only ν_- and they do not produce a relaxation of the proton magnetization toward zero. So when the upper sweep frequency limit passes ν_+ from above, the proton NMR signal increases. For a similar reason the proton NMR signal increases also when the lower sweep frequency limit passes ν_- from below and the upper sweep frequency limit is fixed above ν_+. In such a way ν_+, ν_-, and ν_0 are determined to an accuracy of approximately 10 kHz. Moreover, with this technique it is possible to separate in the complex ^{14}N NQR spectrum the triplets ν_+, ν_-, and ν_0 corresponding to various inequivalent nitrogen positions in the crystal. In the final step of the experiment, during the relaxation period, the condition $\nu_H = \nu_0$ is satisfied and two rf magnetic fields of frequencies ν_1 and ν_2 are applied. When $\nu_1 = \nu_-$ and $\nu_2 = \nu_+$ we observe a relaxation of the proton magnetization toward zero. Performing the scans at the frequencies ν_1 and ν_2, the accuracy of determination of the ^{14}N NQR frequencies is increased to about 5 kHz or better, depending mainly on the magnetic field broadening of the ^{14}N NQR lines during the relaxation period.

DFT/QTAIM CALCULATIONS

Quantum chemical calculations were carried out within the Gaussian 03[33] code run on the CRAY supercomputer at the Poznań Supercomputer and Network Centre (PCSS). All calculations were performed within the density functional theory (DFT) with exchange-correlation hybrid functional: B3LYP (three-parameter exchange functional of Becke B3[34] combined with the Lee−Yang−Parr correlation functional LYP[35]) using the extended basis sets with polarization and diffuse functions 6-311++G(d,p), which has proven to produce highly accurate electron densities and electric field gradient (EFG) tensor.[36] The principal components of second rank symmetric tensor of electric field gradient (EFG), obtained at the 6-311++G(d,p) level of theory assuming optimized and X-ray structures were used to calculate the NQR parameters (quadrupole coupling constants, asymmetry parameters, and frequencies at all nitrogen atoms). The nuclear quadrupole moment for ^{14}N equal to 2.044 fm^2 was assumed.[37]

A theoretical analysis of the intermolecular interactions was performed within the Bader's Quantum Theory of Atoms in Molecules (QTAIM).[38] Within this approach the net atomic charges can be obtained by the integration of the charge distribution within properly defined atomic basins. Additionally, the electron density $\rho(r)$ of a molecule treated as a scalar field can be examined by analysis of its gradient vector field. The values of $\rho(r)$ at start and end points of a gradient path which follows the largest increase in $\rho(r)$ take the extreme points (maxima, saddle points, or minima in the electron density). Depending on the nature of the extreme they are named as core-, bond-, ring-, and cage-critical points and denoted as NACP (nuclear attractor critical point)—local maximum of electron density, BCP (bond critical point)—minimum in the direction of the nucleus but it is a maximum in another main direction RCP (ring critical point)—minimum in two principal axes, and CCP (cage critical point)—local minimum of electron density, respectively. The kind of the extreme was determined with the help of Hessian matrix composed of nine second-order derivatives of $\rho(r)$. The Poincare−Hopf relationship was used as a consistency check. At each extreme point the topological parameters, the electron density and its Laplacian were calculated. Additionally, the ellipticity of the bond, ε, the σ - and π-characters of the bond, the total electron energy density at BCP (H_{BCP}) and its components: the local kinetic energy density (G_{BCP}) and the local potential energy density (V_{BCP}) and hydrogen-bonding energy E_E according to Espinosa ($E_E = {}^1/_2 V_{BCP}$)[39] were calculated at each BCP.

dx.doi.org/10.1021/jp302659k | J. Phys. Chem. B 2012, 116, 8793−8804

EXPERIMENTAL RESULTS AND DISCUSSION

The solid-effect spectra of 2-thiouracil measured at ν_H = 100 kHz and ν_H = 200 kHz are presented in Figure 3. The

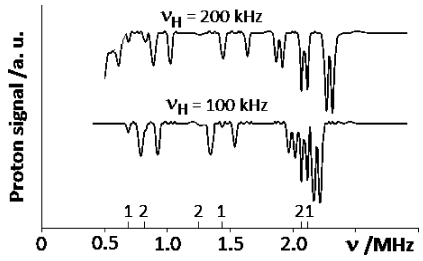

Figure 3. ^{1}H−^{14}N solid effect spectra of 2-thiouracil measured at ν_H = 200 kHz and ν_H = 100 kHz. The temperature of the sample is 295 K. The ^{14}N NQR frequencies from two nonequivalent nitrogen sites labeled as 1 and 2 are shown on the frequency scale.

temperature of the sample was 295 K. The sextet of dips around $\nu \approx 2.1$ MHz clearly shows the presence of two inequivalent nitrogen positions. The positions of the two inner dips, observed at ν_1 = 2.060 MHz and ν_2 = 2.110 MHz are independent of ν_H. They are the level crossing dips at two different ^{14}N NQR frequencies ν_+ equal to $\nu_{+1} = \nu_1$ and $\nu_{+2} = \nu_2$. The two outer pairs of dips, which are shifted away from the level crossing dips on increasing ν_H, are the solid effect dips. The level crossing dips are observed also at two values of ν_0: 680 kHz and 815 kHz. This pair of dips is associated with two solid effect dips at $\nu_0 + \nu_H$. The solid effect dips at $\nu_0 - \nu_H$ are usually not observed. The level crossing dips at two values of ν_-, 1.245 and 1.430 MHz, are weak and are not observed, but the solid effect dips at $\nu_- + \nu_H$ are clearly observed. There are thus two triplets of the ^{14}N NQR frequencies, (2.110, 1.430, 0.680 MHz) and (2.060, 1.225, 0.835 MHz), corresponding to two inequivalent nitrogen positions in the molecule. All molecules in the crystal are thus crystallographically equivalent. The presence of well-expressed level crossing dips shows that the N−H dipolar interaction is strong. Both nitrogen positions are thus the amino positions (−NH−).

The complete set of the ^{14}N NQR frequencies was measured at room temperature and at T = 173 K to check for the presence of possible molecular motions that may influence the NQR spectra. The ^{14}N NQR frequencies ν_+ and ν_-, the quadrupole coupling constants e^2qQ/h and the asymmetry parameters η of the presently measured and some related compounds are presented in Table 1. The ^{14}N NQR frequencies are determined to an accuracy of ±5 kHz.

The temperature coefficient K_T of the ^{14}N quadrupole coupling constant, $K_T = \Delta(e^2qQ/h)/\Delta T$ is observed in the range between −0.49 and +0.41 kHz/K. The negative value of K_T may be associated with molecular librations which partially average the EFG tensor at the position of the nitrogen nucleus. On increasing temperature the intensity of the molecular librations increases, which causes a reduction in the ^{14}N quadrupole coupling constant. The increase in e^2qQ/h with increasing temperature is usually a consequence of a rearrangement of the electron charge distribution that may be in the compounds studied associated with changes in the hydrogen bonds and with changes in the population of the electron orbitals. The temperature variation of the electron charge distribution may of course also be responsible for a negative value of K_T. The negative and positive values of K_T in all

Table 1. The ^{14}N NQR Frequencies ν_+ and ν_-, the Quadrupole Coupling Constants e^2qQ/h and the Asymmetry Parameters η of Presently Measured and Some Related Compounds (Positions in Bold−Final Assignment)

substance	nitrogen position	T [K]	ν_+ [MHz]	ν_- [MHz]	e^2qQ/h [MHz]	η [−]
uracil[17]	1	77	2.320	1.620	2.627	0.533
	3	77	2.285	1.590	2.583	0.538
	1	294	2.300	1.640	2.630	0.502
2-thiouracil	**1**	295	2.110	1.430	2.360	0.576
	1	173	2.110	1.410	2.345	0.597
	3	295	2.060	1.245	2.205	0.740
	3	173	2.060	1.225	2.190	0.763
4-thiouracil	**1**	295	2.165	1.345	2.340	0.701
	1	173	2.165	1.320	2.325	0.727
	3	295	2.145	1.525	2.445	0.507
	3	173	2.145	1.500	2.430	0.531
2,4-dithiouracil[40]	1	301	2.030	1.180	2.140	0.794
	3	301	1.970	1.240	2.140	0.682
6-methyl-uracil[17]	1	77	2.466	1.793	2.839	0.474
	3	77	2.329	1.546	2.583	0.606
6-methyl-2-thiouracil	**1**	295	2.160	1.340	2.335	0.703
	1	173	2.150	1.305	2.305	0.734
	3	295	2.120	1.500	2.415	0.514
	3	173	2.120	1.470	2.395	0.543
6-azauracil	6	295	4.315	4.275	5.725	0.014
	6	173	4.360	4.320	5.785	0.014
	1	295	3.460	1.900	3.575	0.873
	1	173	3.470	1.935	3.605	0.852
	3	295	2.200	1.500	2.465	0.568
	3	173	2.200	1.550	2.500	0.520
thymine[17]	**1**	77	2.431	1.694	2.750	0.536
	3	77	2.313	1.648	2.641	0.504
Thymine[41]	3	181	2.300	1.420	2.490	0.71
6-aza-thymine[42]	3*	RT	2.180	1.500	2.453	0.554
6-aza-2-thiothymine	6	295	4.280	3.780	5.375	0.186
	6	173	4.305	3.813	5.410	0.182
	1	295	3.170	1.710	3.255	0.898
	1	173	3.170	1.690	3.240	0.914
	3	295	2.080	1.320	2.265	0.671
	3	173	2.050	1.270	2.215	0.705

investigated compounds are of the same order of magnitude and relatively small. This excludes the presence of strong molecular motions and electron charge redistributions by varying temperature. This conclusion is in agreement with the small temperature variation of proton T_1 observed during the NQDR measurements.

The difference in the two ^{14}N quadrupole coupling constants assigned to the two inequivalent nitrogen positions 1 and 3 in 2-thiouracil, 4-thiouracil and 6-methyl-2-thiouracil, Table 1, is small. It is therefore difficult to assign unambiguously the ^{14}N NQR parameters to the particular positions 1 and 3 in each of these compounds only on the basis of simple arguments. The situation is different in the aza-compounds, for which the differences between the three ^{14}N NQR parameters, especially quadrupole coupling constants, are large. On the basis of the literature data it is possible to assign the highest quadrupole coupling constant to the imino nitrogen position in the azo

dx.doi.org/10.1021/jp302659k | J. Phys. Chem. B 2012, 116, 8793−8804

Table 2. ^{14}N NQR Frequencies, Quadrupole Coupling Constants and Asymmetry Parameters η, the Sum of σ and π Character of N−C and N−N Bonds at Each Nitrogen Site Calculated for the Compounds Studied (Trimers) at B3LYP/6-311++G** Level

compound	site	ν_+ [MHz]	ν_- [MHz]	ν_0 [MHz]	e^2qQ/h [MHz]	η [−]	σ^j	π^j
6-azauracil[a]	N(1)	3.957	2.451	1.506	4.272	0.705	1.3255	−3.0007
	N(3)	2.554	1.664	0.890	2.812	0.633	0.8015	−2.6390
	N(6)	4.782	4.700	0.082	6.321	0.026	1.7937	−3.0891
6-aza-2thiotymine[b]	N(1)	3.852	2.154	1.698	4.004	0.848	1.3654	−2.9493
	N(3)	2.582	1.429	1.152	2.674	0.862	0.7848	−2.5963
	N(6)	4.695	4.018	0.677	5.809	0.233	1.7685	−3.1211
uracil[c]	N(1)	2.726	1.812	0.914	3.025	0.604	0.8329	−2.5783
	N(3)	2.654	1.606	1.048	2.840	0.738	0.7660	−2.6062
thymine[d]	N(1)	2.949	1.667	1.282	3.077	0.833	0.7670	−2.5207
	N(3)	2.687	1.543	1.144	2.820	0.811	0.7278	−2.5550
2-thiouracil[e]	N(1)	2.460	1.726	0.734	2.791	0.526	0.8215	−2.5702
	N(3)	2.455	1.512	0.943	2.645	0.713	0.7364	−2.5493
2-thiouracil[f]	N(1)	2.621	1.846	0.776	2.978	0.521	0.7358	−2.4583
	N(3)	2.459	1.270	1.190	2.486	0.957	0.6987	−2.4629
2,4-dithiouracil[g]	N(1)	2.626	1.735	0.891	2.907	0.613	0.7976	−2.4599
	N(3)	2.550	1.434	1.116	2.656	0.840	0.9300	−2.6232
6-methyl-2-thiouracil[h]	N(1)	2.667	1.677	0.990	2.896	0.684	0.7997	−2.5593
	N(3)	2.623	1.564	1.059	2.791	0.759	0.7520	−2.5448
4-thiouracil[i]	N(1)	2.641	1.618	1.023	2.839	0.721	0.7446	−2.5004
	N(3)	2.660	1.782	0.878	2.961	0.593	0.7137	−2.4591

[a]X-ray structure from ref 43. [b]X-ray structure from ref 44. [c]X-ray structure from ref 45. [d]X-ray structure from ref 46. [e]X-ray structure from ref 47. [f]Structure predicted. [g]X-ray structure from ref 48. [h]X-ray structure from ref 49. [i]No X-ray data available, structure predicted. [j]σ,π: sum of σ and π characters of N−C and N−N (aza) bonds; negative sign results from Hessian.

group which is in the hydrazone (=N−NH−) form. The intermediate quadrupole coupling constant corresponds to the amino nitrogen position in the azo group, whereas the smallest quadrupole coupling constant corresponds to the amino (−NH−) nitrogen position 3. The validity of this assignment in the aza-compounds is confirmed by the calculations performed assuming the monomers as well as clusters (trimers) built, using X-ray data at the B3LYP/6-311++G(d,p) level Table 2, Figure 4a.

A reliable assignment of the frequencies to particular nitrogen sites in 2-thiouracil, 4-thiouracil, and 6-methyl-2-thiouracil requires taking into account weak electronic effects, intermolecular interactions, and tautomerism capable of modifying the type of site due to proton migrations. However, the number of lines suggests that there is one tautomeric form in each case. The latter seems to be consistent with the X-ray data[47,49] according to which 2-thiouracil and 6-methyl-2-thiouracil crystallizes in triclinic $P-1$ and monoclinic $P21/c$ space groups with 4 and 2 equivalent molecules in elementary cells, respectively. The calculations performed assuming the monomer (X-ray data) at the B3LYP/6-311++G(d,p) level Table 2, Figure 4a revealed a discrepancy between the experiment and results of calculations. Two higher NQR frequencies ν_+, ν_- and e^2Qqh^{-1} are overestimated, while the lowest NQR frequency ν_0 and η are underestimated. Thus an attempt to determine the tautomer in solid state on the basis of NQR parameters calculated assuming a single molecule can be highly misleading, but the assumption of a cluster consisting of tautomers reflecting intermolecular interactions provides a reliable result. The correlation between the experimentally determined NQR parameters and the calculated ones under the assumption of trimers built of the most stable oxo-thione form (stability order oxo-thione ≫ oxo-thiol ≫ hydroxy-thiol ≫ hydroxy-thione) is very good, Table 2, Figure 4b.

The influence of temperature factor is negligible (correlation coefficient, standard deviation, and slope are 0.9930, 0.7237 MHz, and 1.075 at 173 K and 0.7041, 0.9932 MHz, and 1.083 at 193 K).

As the X-ray data for 4-thiouracil are not available, the hypothetical trimer linked by N−H···O and N−H···S bonds, Figure 5a, was constructed on the basis of X-ray data for 2-thiouracil and 2,4-dithiouracil and fully optimized. The NQR parameters for 4-thiouracil are very well reproduced by B3LYP/6-311++G(d,p) calculations performed under the assumption of the predicted trimer consisting of oxo-thione forms 4-T(1), Figure 5a. For the sake of comparison, the hypothetical trimer of 2-thiouracil was optimized and the geometry was compared to that of the X-ray one. In this case the rms factor is small (0.15 Å, Figure 5b), and the reproduction of NQR parameters is very good (Table 2, correlation coefficient 0.980, standard deviation 0.163), which confirms the validity of this approach. The quality of reproduction of ^{14}N NQR parameters by DFT obtained assuming the two possible assignments in 4-thiouracil is comparable (the correlation coefficients are 0.991 and 0.959 and the standard deviations are 0.102 and 0.215 MHz) and the opposite assignment is suggested on the basis of trimer and monomer analysis. The reason for this effect is the participation of N(1) in a weak N(1)-H···S and N(3) in a strong N(3)-H···O bond, which results in the 4-thiouracil opposite assignment, rather than that observed in 2-thiouracil in which N(1) participates in a strong N(1)-H···O and N(3) participates in a weak N(3)-H···S bond.

The QTAIM approach allows description of the molecular topology of intermolecular bonds in terms of BCPs, Table 3. The values of electron densities at BCP, $\rho_{BCP}(r)$, for all N−H···S of 0.0136−0.0251 and N−H···O of 0.0176−0.0495 au and only apart 4-thiouracil fall within a certain range, typically between 0.001 and 0.035 au. The corresponding Laplacian values $\Delta\rho_{BCP}$(N−H···S) and $\Delta\rho_{BCP}$(N−H···O) are positive and

dx.doi.org/10.1021/jp302659k | J. Phys. Chem. B 2012, 116, 8793−8804

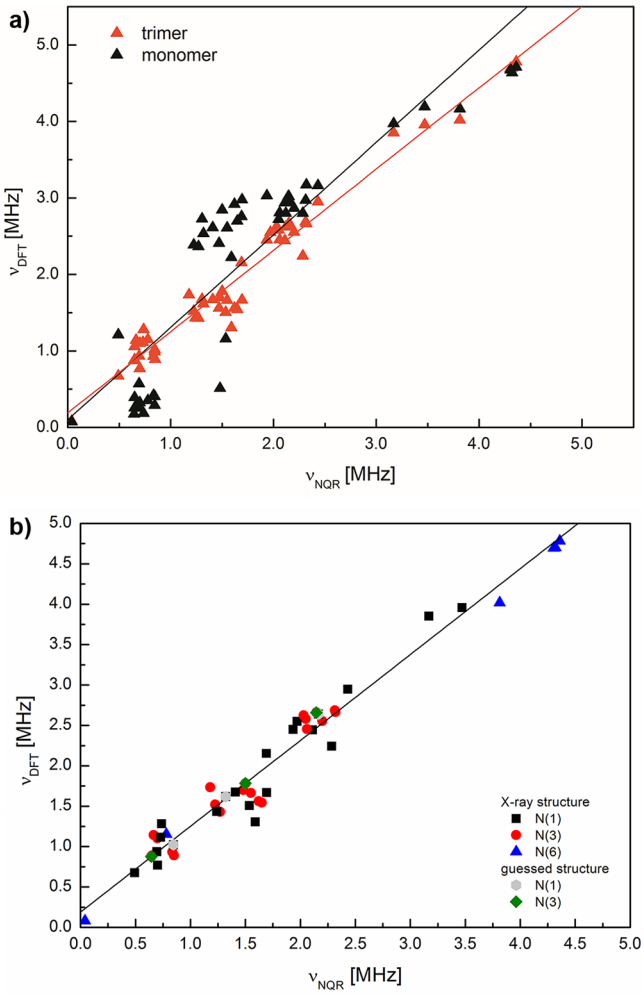

Figure 4. (a) Correlation between the experimental and DFT calculated ^{14}N NQR frequencies: (red) trimers (correlation coefficient, 0.982; curve fit standard deviation, 0.206 MHz), (black) monomers (correlation coefficient 0.895, curve fit standard deviation 0.626 MHz). Solid lines represent linear fit. (b) Correlation between the experimental and DFT calculated ^{14}N NQR frequencies using known crystal structures for the majority of compounds and guessed crystal structure for 4-thiouracil (solid line, linear fit; correlation coefficient, 0.982; curve fit, standard deviation 0.182 MHz).

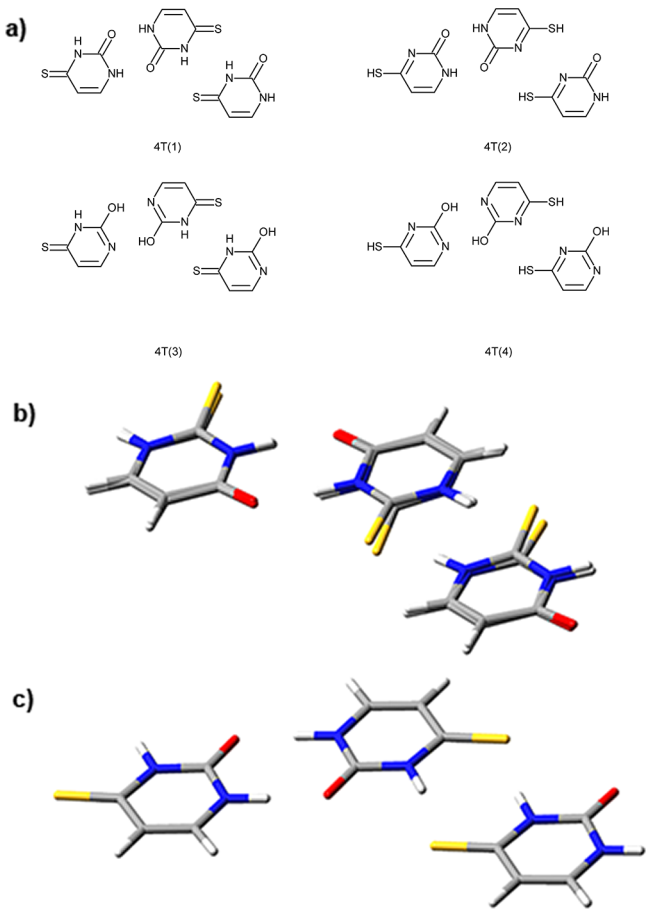

Figure 5. (a) Possible structural patterns of solid 4-thiouracil taking into account formal migrations of protons (stability order: oxo-thione 4-T(1) ≫ oxo-thiol 4-T(2) ≫ hydroxy- thiol 4-T(3) ≫ hydroxy-thione 4-T(4)). (b) Comparison of X-ray and predicted by DFT structures of 2-thiouracil (c) predicted structural pattern of solid 4-thiouracil.

reach 0.0402−0.0506 au and 0.0805−0.1436 au, respectively, typically between 0.006 and 0.130 au. Thus the Koch and Popelier's[50] topological criteria required for HB allow their classification as hydrogen bonds. Close to zero values of $\rho(r)$, small and positive values of Laplacian, relatively high values of ε, nearly zero values of total energy density H_{BCP}, and the values of $|V_{BCP}|/G_{BCP} > 1$ classify the hydrogen bonds in 2-thiouracil and 4-thiouracil as the transit closed-shell. Very small values of $\rho(r)$, small and positive values of Laplacian, relatively high values of ε, and nearly zero values of H_{BCP} and values of $|V_{BCP}|/G_{BCP} \leq 1$ classify the intermolecular interactions in the remaining compounds as the pure closed-shell. It is worth noting that for N−H···S bonds the H···S distance exceeds 2.2 Å (Table 3) thus within the classification by Jeffrey[51] they are considered to be weak and mainly electrostatic, while for N−H···O bonds the situation is the opposite, thus they are considered to be moderate and partially covalent. The electron densities at BCP, corresponding Laplacian values and hydrogen-bond energy E_E estimated using Espinosa formalism, supports the differentiation between stronger N−H···O and weaker N−H···S bonds, Table 3, Figure 6 a,b. Note the characteristic different slopes for particular groups with N−H···O and N−H···S bond types. For thiouracil derivatives a general trend is that the stronger the hydrogen bond is, the lower is the asymmetry parameter (Tables 1,2). For thymine and 6-aza-2-thiotymine, the opposite trend is observed, but this is a result of substitution with hyperconiugative methyl group in para to oxygen and meta to both nitrogen atoms N(1) and N(3). The relief maps of the Laplacian of electron density in the plane of intermolecular H-bonds for the compounds studied, Figure 6c, clearly exhibits maxima in the negative Laplacian on either side of the nitrogen atoms, corresponding to the lone pair model. Moreover, they show the polarization of the nitrogen lone-pair electrons toward hydrogen and differences in polarization of the nitrogen lone-pairs in N−N and N−C. Considering the topology of the fragments with nitrogen atoms, the aromatic C−N bonds within the heterocyclic ring are of similar strength, with small ranges of values of electron density ρ_{BCP}(C−N), its Laplacian $\Delta\rho_{BCP}$(C−N), and delocalization index δ(C,N) (0.299−0.327, −0.90−0.093, and 0.92−0.97 au, respectively) for all compounds studied. The aromatic N−N bonds are much stronger, with ρ_{BCP} values of 0.363 au, $\Delta\rho_{BCP}$(C−N) values of −0.697 au, and δ(C,N) values of 1.336 au.

dx.doi.org/10.1021/jp302659k | J. Phys. Chem. B 2012, 116, 8793−8804

Table 3. Topological Parameters of $\rho(r)$ for Selected[a] Hydrogen Bonds in Uracil/Thiouracil Analogues (the Hydrogen-Bond Length R(X−H···Y), the Proton-Donor Distance R(N−H), the Proton-Acceptor Distance R(H···Y), Y = S or O; Electron Density at BCP ($\rho_{BCP}(r)$), Its Laplacian $\Delta_{BCP}(\rho)$, the Potential Electron Energy Density (V_{BCP}), the Kinetic Electron Energy Density (G_{BCP}), the Total Electron Energy Density (H_{BCP}), and Estimated Hydrogen-Bonding Energy According to Espinosa E_E Calculated at the B3LYP/6-311++G(d,p) Level of Theory

compound	critical point type	R (X−H···Y) [Å]	R(N−H) [Å]	R(Y···H) [Å]	ρ_{BCP} (r) [au]	Δ_{BCP} $\rho(r)$ [au]	ε [−]	V_{BCP} [au]	G_{BCP} [au]	H_{BCP} [au]	$\lvert V_{BCP}\rvert/$ G_{BCP} [−]	E_E [kJ/mol]
6-azauracil[b]	N(1) H···O	2.859	1.025	1.875	0.0282	0.1057	0.0142	−0.0221	0.0243	0.0022	0.909	−28.99
	N(3) H···O	2.8340	0.918	1.928	0.0236	0.1044	0.0409	−0.0187	0.0224	0.0037	0.835	−24.53
6-aza-2-thiothymine[c]	N(1) H···S	3.317	0.820	2.098	0.0148	0.0463	0.0899	−0.0078	0.0097	0.0019	0.804	−10.23
	N(3) H···O	2.876	0.791	2.085	0.0176	0.0805	0.0589	−0.0125	0.0163	0.0038	0.767	−16.40
uracil[d]	N(1) H···O	2.864	0.836	2.039	0.0201	0.088	0.0744	−0.0149	0.0184	0.0036	0.810	−19.55
	N(3) H···O	2.865	0.877	1.995	0.0222	0.092	0.0589	−0.0166	0.0198	0.0032	0.838	−21.78
thymine[e]	N(1) H···O	2.827	0.822	1.955	0.0212	0.0967	0.0717	−0.0162	0.0202	0.0040	0.802	−21.25
	N(3) H···O	2.833	0.880	2.004	0.0239	0.1011	0.0575	−0.0186	0.0219	0.0034	0.849	−24.40
2-thiouracil[f]	N(1) H···S	3.299	1.030	2.284	0.0251	0.0506	0.0585	−0.0142	0.0134	−0.0008	1.060	−18.63
	N(3) H···O	2.819	1.030	1.794	0.0351	0.1174	0.0320	−0.0294	0.0294	−0.00001	1.000	−38.57
2-thiouracil[g]	N(1) H···S	3.346	1.035	2.330	0.0233	0.0472	0.0497	−0.0125	0.0122	−0.0003	1.030	−16.44
	N(3) H···O	2.733	1.049	1.672	0.0451	0.1391	0.0262	−0.0422	0.0385	−0.0037	1.096	−55.36
2,4-dithiouracil[h]	N(1) H···S	3.334	0.980	2.426	0.019	0.0461	0.0678	−0.0099	0.0107	0.0008	0.925	−12.99
	N(3) H···S	3.314	0.946	2.394	0.0195	0.0492	0.0494	−0.0106	0.0115	0.0009	0.922	−13.90
6-methyl- 2-thiouracil[I]	N(1) H···O	2.786	0.955	1.852	0.0294	0.1209	0.0284	−0.025	0.0276	0.0026	0.906	−32.79
	N(3) H···S	3.419	0.885	2.546	0.0136	0.0402	0.0650	−0.0067	0.0084	0.0017	0.798	−8.79
4-thiouracil[j]	N(1) H···O	2.709	1.051	1.661	0.0495	0.1436	0.0384	−0.0477	0.0418	−0.0059	1.141	−62.57
	N(3) H···S	3.342	1.038	2.319	0.0237	0.048	0.0427	−0.0129	0.0124	−0.0005	1.040	−16.92

[a]Only those linking N(1) and N(3) sites with O and S are listed. [b]X-ray structure from ref43. [c]X-ray structure from ref 44. [d]X-ray structure from ref 45. [e]X-ray structure from ref 46. [f]X-ray structure from ref 47. [g]Structure predicted. [h]X-ray structure from ref 48. [I]X-ray structure from ref 49. [j]no X-ray data available, structure predicted.

When limiting the analysis of topology of electron density to local effects in the heterocyclic ring only, a correlation between the experimentally determined quadrupole coupling constant e^2qQ/h and η and the DFT/QTAIM calculated sum of σ and π characters of N−C and N−N bonds (Figure 6 d,e) becomes easily apparent. Note the characteristic different slopes for particular groups with different bond types N−C and N−N (aza). Although distinction between σ- and π-bonds is not relevant when QTAIM approach is used, it is appealing to describe EFG tensor features within the σ/π model.

Several studies[52] have shown that all the principal values of the ^{14}N quadrupole coupling tensor are intercorrelated. These correlations are helpful in the experimental search for the ^{14}N NQR frequencies and in assignment of a quadrupole coupling tensor to a particular nitrogen position. The correlations reflect the strength of the inter- and intramolecular interactions. It is thus interesting to check whether these correlations are observed also for the amino- and iminonitrogen positions in the heterocyclic compounds. Figure 7 presents the correlation of q_{XX} and q_{YY} versus q_{ZZ} for the planar amino groups C−NH−C, N−NH−C, and C−NR−C, where R starts with C, for several heterocyclic compounds. The present experimental data were supplemented with those for pure and substituted thymine, uracil, uridine, barbituric acid, orotic acid, and cyanuric acid,[53] cytosine, adenine, hypoxanthine, and guanine,[54] 4-*N*-cytosine derivatives,[20] and 2-nitro-5-methylimidazole derivatives.[21]

The data for the C−NH−C group show a linear correlation between q_{XX} and q_{ZZ} and between q_{YY} and q_{ZZ}. The two correlation lines are nearly parallel with the slope $\Delta q_{XX}/\Delta q_{ZZ} = \Delta q_{YY}/\Delta q_{ZZ} = -0.5$ and can be expressed as

$$q_{XX} = -0.5q_{ZZ} + 0.75 \text{ MHz}$$
$$q_{YY} = -0.5q_{ZZ} - 0.75 \text{ MHz} \quad (6)$$

What varies in this correlation is an axially symmetric contribution to the EFG tensor with the highest principal value along the Z axis. As already concluded by Garcia and Smith[21] for such aromatic compounds in which the lone pair of electrons contributes to the π-electron system, the population of the nitrogen π-electron orbital varies depending on the hydrogen bonding and ring substitutions. This variation induces changes in the axially symmetric contributions to the EFG tensor with the symmetry axis along the normal to the plane of the amino group. The Z-principal axis of the EFG tensor is thus perpendicular to the plane of the amino group.

There are less data for the N−NH−C and C−NR−C groups but the diagram suggests that through the points corresponding to these groups the lines parallel to the correlation lines observed for the C−NH−C group can be plotted. On the one hand, the substitution of H by C decreases the difference between q_{XX} and q_{YY}, but on the other hand, the substitution of C by N increases the difference between q_{XX} and q_{YY}. This can be easily understood in a simple model. The three functional groups are presented in Figure 7. In the simple model we assume that the functional groups are planar and that the three R′−N−R″ angles in a group are equal 120°. The contribution to the quadrupole coupling tensor from the π-orbital is assumed to be axially symmetric with the symmetry axis perpendicular to the plane of the functional group (z-axis), whereas the contribution to the quadrupole coupling tensor from a σ-bond is assumed to be axially symmetric with the symmetry axis along the bond.

dx.doi.org/10.1021/jp302659k | J. Phys. Chem. B 2012, 116, 8793−8804

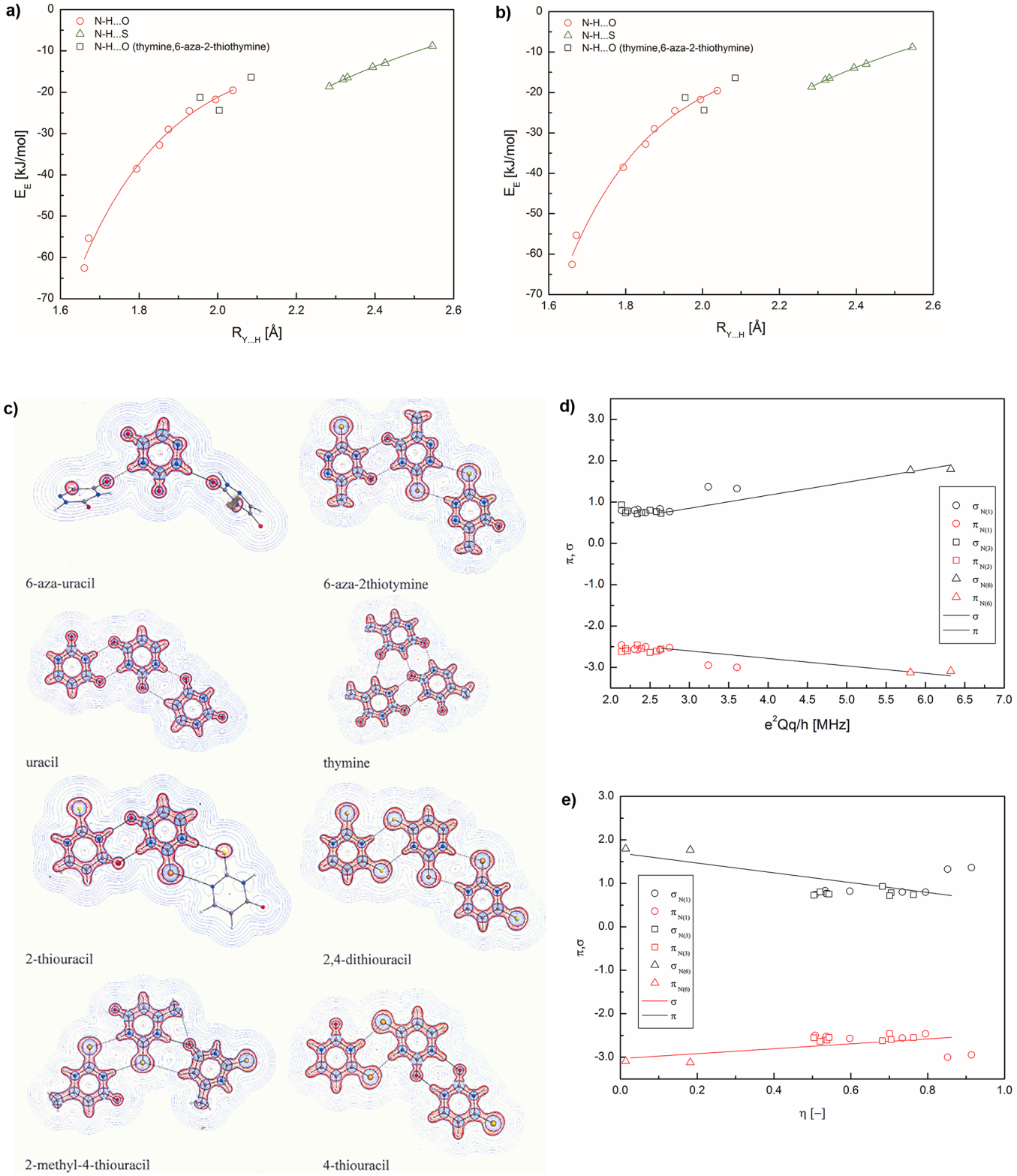

Figure 6. (a) The hydrogen-bond strength E_E, (b) electron density $\rho_{BCP}(r)$, and its Laplacian $\Delta_{BCP}(\rho)$ versus proton-acceptor H···Y distance (solid lines, exponential fit); (c) the Laplacian contours in the compounds studied (negative regions in red, positive regions in blue); (d) DFT calculated sum of σ and π character of N−C; and (e) N−N bonds at each nitrogen site N(1), N(3), or N(6) (solid lines, trends; scattered points, aza derivatives).

The ^{14}N quadrupole coupling tensor q in a C−NR−C group is in the above model the sum of an axially symmetric σ contribution and an axially symmetric π contribution both with the symmetry axis along the z axis. The difference $q_{XX} - q_{YY}$ and the asymmetry parameter η, $\eta = (q_{XX} - q_{YY})/q_{ZZ}$, are expected to be zero. The experimentally observed asymmetry parameter η is not zero, as expected in this model, but it is small. The reason for a nonzero asymmetry parameter η may be

dx.doi.org/10.1021/jp302659k | J. Phys. Chem. B 2012, 116, 8793−8804

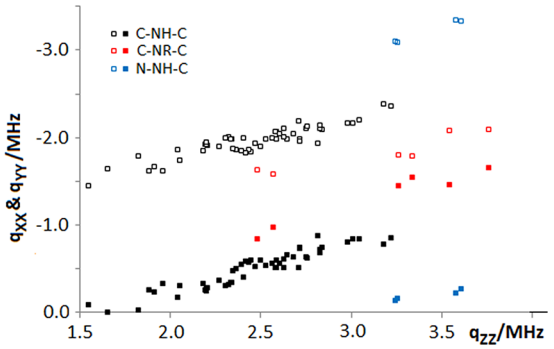

Figure 7. Correlation between q_{YY} (open symbols), q_{XX} (solid symbols), and q_{ZZ} in secondary amino groups C−NH−C and N−NH−C and in tertiary amino groups C−NR−C, where R starts with C, for several heterocyclic compounds.

the deviation of the angles between the σ bonds from 120° and a slight inequivalence of the three C−N σ bonds. Indeed, for example, for 1-methyluracil and 3-methyluracil the angle is 121.40° and 125.40°, respectively, while the C−N bond lengths are 1.371, 1.377, and 1.460 Å; 1.400, 1.405, and 1.461 Å, respectively.

When a carbon atom is exchanged by a less electronegative hydrogen atom (N−C → N−H), as in a C−NH−C group, we expect a shift of the electron charge in the σ bond toward nitrogen. In the ^{14}N quadrupole coupling tensor for the C−NH−C group we must add to the axially symmetric quadrupole coupling tensor an axially symmetric contribution δq_{CH} with the symmetry axis along the y axis and with the negative largest principal value $-x_{CH}$:

$$\delta q_{CH} = \begin{bmatrix} x_{CH}/2 & 0 & 0 \\ 0 & -x_{CH} & 0 \\ 0 & 0 & x_{CH}/2 \end{bmatrix} \quad (7)$$

This contribution causes an increase in the difference $q_{XX} - q_{YY}$ by $3x_{CH}/2$. From the data given in Figure 7 we estimate x_{CH} as approximately 0.9 MHz. Assuming that a single 2p electron in the nitrogen atom generates an axially symmetric contribution to the quadrupole coupling tensor with the largest principal value q_0 equal −9 MHz,[19] the value of x_{CH} corresponds to a shift of about 0.1 electron charge toward the nitrogen atom.[19]

The quadrupole coupling constant of a C−NH−C group varies between 1.5 and 3.3 MHz, which corresponds to the variation in the population of the π-electron orbital equal (3.3 − 1.5 MHz)/9 MHz = 0.2. The N−C bond length varies from 1.351 to 1.377 Å, while the <CNC angle varies from 122.69° to 125.40°.

When in addition a carbon atom is replaced by a more electronegative nitrogen atom, as in the C−NH−N group, the electron charge is partially shifted from the amide nitrogen atom to the imide nitrogen atom. The change δq_{CN} in the quadrupole coupling tensor at the amide nitrogen position is an axially symmetric tensor with the symmetry axis along the N−N bond and with the highest principal value x_{CN}, which is in this case positive. The change δq_{CN} is in the coordinate system given in Figure 8 expressed as

$$\delta q_{CH} = \begin{bmatrix} 5x_{CN}/8 & 3\sqrt{3}x_{CN}/8 & 0 \\ 3\sqrt{3}x_{CN}/8 & -x_{CH}/8 & 0 \\ 0 & 0 & -x_{CN}/2 \end{bmatrix} \quad (8)$$

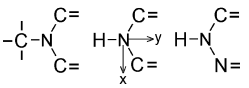

Figure 8. The C−NR−C, C−NH−C, and N−NH−C functional groups and the coordinate system used in the calculations. The hydrogen atoms bonded to the −C= carbon positions are not shown.

The difference in the two smaller principal values of the quadrupole coupling tensor for the amino nitrogen position in the C−NH−N group is equal to

$$q_{XX} - q_{YY} = \frac{3}{2}\sqrt{x_{CH}^2 + x_{CN}^2 + x_{CH}x_{CN}} \quad (9)$$

From Figure 7 we estimate this difference as being of 3 MHz. Since x_{CH} is known, it is possible to calculate x_{CN} from expression (9) as x_{CN} = 1.4 MHz. This value corresponds to a shift of 0.15 electron charge from the amino nitrogen to the imino nitrogen. It is interesting that the ratio x_{CH}/x_{CN} = 0.64 is close to the ratio of the electronegativity differences $(\chi_C - \chi_H)/(\chi_N - \chi_C)$ = 0.71. In aza compounds N−N bond length is only 1.351 Å, while the <CNN angle is only 117.86°.

The imino nitrogen can be treated in a similar way. Figure 9a shows the correlation of q_{XX} and q_{YY} versus q_{ZZ} for the C−N= C nitrogen positions in substituted imidazole and for the N−N=C nitrogen positions. The data for imidazole are taken from refs 19 and 21. The data for the N−N=C functional groups are those obtained in this study plus the data taken from refs 24 and 53.

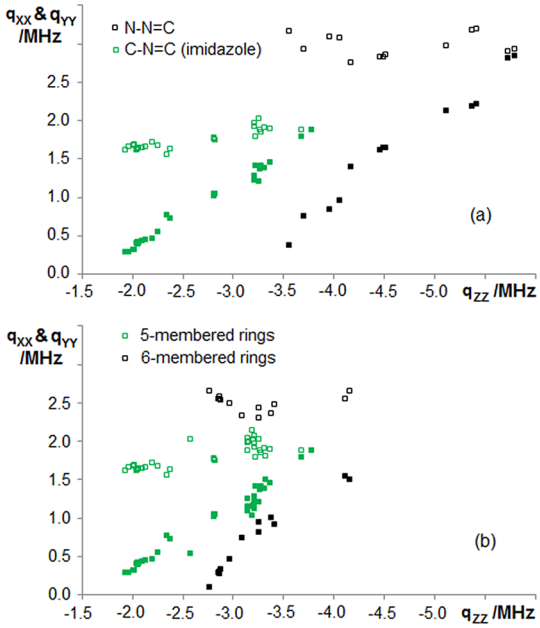

Figure 9. The correlation of the principal values q_{XX} and q_{YY} versus q_{ZZ} for the N−N=C functional groups and C−N=C functional groups in imidazole (a) and for the C−N=C functional groups in five- and six-membered rings.

dx.doi.org/10.1021/jp302659k | J. Phys. Chem. B 2012, 116, 8793−8804

Figure 9a reveals a characteristic feature of this correlation. One of the principal values (in the present case q_{YY}) exhibits a weak variation in q_{ZZ}. For the N−N=C group, q_{YY} is on average 2.9 MHz, whereas for imidazole it is on average 1.7 MHz. A similar situation has been observed also in pyridine[54,55] where q_{XX} varies weakly with respect to q_{ZZ} and q_{YY}. A reasonable explanation of this feature is that the electron electric charge exchanges between the lone pair orbital and the π-electron orbital under the influence of hydrogen bonding and ring substitution, whereas the total population remains constant. The principal axis Y lies in the molecular plane and is perpendicular to the lone pair orbital. The correlation of the NQR data for the N−N=C functional group from various five- and six-membered rings displays a reasonably small scattering of data points. On the other hand, the scattering is greater for the C−N=C functional group. Figure 9b presents the correlation of q_{XX} and q_{YY} versus q_{ZZ} for the C−N=C functional group in the five- and six-membered rings. The data are taken for substituted imidazole,[19,21] substituted benzimidazole,[23] purines, and cytosine derivatives.[18,20,22,16,25,15] The data show a clear distinction between the five- and six-membered rings that is presumably the effect of different bond angles (in five-membered ring bond angles typically vary from 104° to 107°, in six-membered ring bond angles vary from 120° to 126°) and delocalization of π-electrons and lone pair electrons. In the six-membered rings the slowly varying principal value of the quadrupole coupling tensor q_{YY} is on average of about 2.5 MHz and in five-membered rings it is of about 1.8 MHz. On the other hand, in substituted pyridine the slowly varying principal value of the quadrupole coupling tensor q_{XX} is only of about 1.3 MHz.

CONCLUSIONS

The ^{14}N NQR spectra of 2-thiouracil, 4-thiouracil, 6-methyl-2-thiouracil, 6-azauracil, and 6-aza-2-thiothymine have been measured by ^{1}H−^{14}N double resonance at 173 and 295 K. The ^{14}N NQR frequencies have been assigned to particular nitrogen sites on the basis of experimental and theoretical arguments following from the Density Functional Theory (DFT)/Quantum Theory of Atoms in Molecules (QTAIM).

The changes in the molecular skeletons, electric charge distribution, intermolecular interactions pattern, and molecular aggregations caused by oxygen replacement with sulfur and carbon replacement with nitrogen have been studied theoretically by DFT/QTAIM in the presently investigated thio- and aza-compounds and in some other related compounds, whose ^{14}N NQR spectra have been previously measured. It is shown that an attempt to determine the tautomer in solid state on the basis of NQR parameters calculated assuming a single molecule can be highly misleading, but the assumption of a cluster consisting of tautomers reflecting intermolecular interactions provides a reliable result.

A correlation of the principal values of the quadrupole coupling tensor at the amino nitrogen positions in heterocyclic rings has been observed. The variation in the NQR parameters is mainly related to the variation in the population of the π-electron orbital. The effect of substitution of a carbon atom bound to amino nitrogen by a less electronegative hydrogen atom or by a more electronegative nitrogen atom on the ^{14}N quadrupole coupling tensor of the amino nitrogen has been analyzed. A correlation of the principal values of the quadrupole coupling tensor has been also observed at the imino nitrogen positions in heterocyclic rings. It is shown that the ^{14}N NQR data from the imino nitrogen positions can be used to differentiate between five- and six-membered rings. The effect of carbon substitution by nitrogen (C−N=C → N−N=C) on the quadrupole coupling tensor has been investigated.

For thiouracil derivatives a general trend is that the stronger the hydrogen bond is, the lower the asymmetry parameter is, while for thymine and 6-aza-2-thiothiotymine, the opposite trend is observed, being a result of substitution with the hyperconiugative methyl group in para to oxygen and meta to both nitrogen atoms N(1) and N(3). The N−H···S bonds have been found weak and mainly electrostatic, while N−H···O bonds have been found moderate and partially covalent.

This study also demonstrates the advantages of combining NQR and DFT/QTAIM to predict a crystalline structure. As the X-ray data for 4-thiouracil are not available, a hypothetical trimer linked by N−H···O and N−H···S bonds is constructed on the basis of X-ray data for 2-thiouracil and 2,4-dithiouracil and fully optimized. The ^{14}N NQR parameters for 4-thiouracil are very well reproduced by B3LYP/6-311++G(d,p) calculations performed under the assumption of the predicted trimer. The quality of the known structure of 2-thiouracil predicted using the same technique was high (rms = 0.15 Å).

The advantages of using a combination of NQR and DFT methods for the analysis of electric charge distribution and intermolecular interactions in biological and organic molecules are demonstrated.

AUTHOR INFORMATION

Notes

The authors declare no competing financial interest.

ACKNOWLEDGMENTS

Generous allotment of computer time from the Poznan Supercomputing and Networking Center (PCSS) in Poznań, Poland is gratefully acknowledged.

REFERENCES

(1) Beck, F.; Howlett, G. J. *J. Mol. Biol.* **1977**, *111*, 1−17.
(2) Astwood, E. B. *J . Am. Med. Assoc.* **1943**, *122*, 78−81.
(3) Astwood, E. B. *The Pharmacological Basis of Therapeutics*; Goodman, L. S., Gilman, A., Eds.; Macmillan: Toronto, 1970; p 1538.
(4) Brockman, R. W.; Anderson, E. P. *Metabolic Inhibitors*; Rochstel, M., Quastel, J. H., Eds.; Academic Press: New York, 1963; pp 239−240.
(5) Komeda, K.; Iwamoto, S.; Kominami, S.; Ohnishi, T. *Photochem. Photobiol.* **1997**, *65*, 115−118.
(6) Handschumacher, R. E.; Welch, A. D. *Cancer Res.* **1956**, *16*, 965−969.
(7) Welch, A. D.; Handschumacher, R. E.; Jaffe, J. J. *Pharmacol. Exp. Ther.* **1960**, *129*, 262−270.
(8) Kuramochi, H.; Kobayashi, T.; Suzuki, T.; Ichimura, T. *J. Phys. Chem. B* **2010**, *114*, 8782−8789.
(9) Besic, E. *J. Mol. Struct.* **2009**, *917*, 71−75.
(10) Favre, A.; Saintome, C.; Fourrey, J. L.; Clivio, P.; Laugaa, P. *Photobiol. B* **1998**, *42*, 109−124.
(11) Favre, A. In *Bioorganic Photochemistry: Photochemistry and the Nucleic Acids*; Morrison, H., Ed.; Wiley: New York, 1990; Vol. *1*, pp 379−425.
(12) Meisenheimer, K. M.; Koch, T. H. *Crit. Rev. Biochem. Mol. Biol.* **1997**, *32*, 101−140.
(13) Sankovic, K.; Krilov, D.; Herak, J. N. *Radiat. Res.* **1991**, *128*, 119−124.
(14) Herak, J. N.; Sankovic, K.; Krilov, D.; Huttermann, J. *Radiat. Res.* **1991**, *151*, 319−324.

(15) Latosińska, J. N.; Seliger, J.; Žagar, V.; Burchardt, D. V. *J. Mol. Model.* **2012**, *18*, 11−26.
(16) Latosińska, J. N.; Seliger, J.; Žagar, V.; Burchardt, D. V. *J. Phys. Chem. A* **2009**, *113*, 8781−8790.
(17) Subbarao, S. N.; Bray, P. J. *J. Chem. Phys.* **1977**, *67*, 1085−1090.
(18) Garcia, M. L. S.; Smith, J. A. S. *J. Chem. Soc. Perkin. Trans. II* **1983**, 1401−1408.
(19) Ashby, C. I. H.; Cheng, C. P.; Brown, T. L. *J. Am. Chem. Soc.* **1978**, *100*, 6057−6063.
(20) Latosińska, J. N.; Seliger, J.; Grechishkin, V.; Spychala, J. *Magn. Reson. Chem.* **1999**, *37*, 881−884.
(21) Latosińska, J. N.; Seliger, J.; Nogaj, B. *Magn. Reson. Chem.* **1999**, *37*, 878−880.
(22) Latosińska, J. N.; Latosińska, M.; Seliger, J.; Žagar, V.; Kazimierczuk, Z. *Chem. Phys. Lett.* **2009**, *476*, 293−302.
(23) Latosińska, J. N.; Latosińska, M.; Seliger, J.; Žagar, V.; Maurin, J. K.; Orzeszko, A.; Kazimierczuk, Z. *J. Phys. Chem. A* **2010**, *114*, 563−575.
(24) Seliger, J.; Žagar, V.; Latosińska, J. N. *Phys. Chem. Chem. Phys.* **2010**, *12*, 13007−13019.
(25) Latosińska, J. N.; Latosińska, M.; Tomczak, M. A.; Seliger, J.; Žagar, V. *J. Mol. Model.* **2011**, *17*, 1781−1800.
(26) Seliger, J. Nuclear quadrupole resonance. Theory. In *Encyclopedia of Spectroscopy and Spectrometry*; Lindon, J. C., Tranter, G. E., Holmes, J. L., Eds.; Academic Press: San Diego, CA, 2000; pp 1672−1680.
(27) Seliger, J. *Appl. Magn. Reson.* **2012**, DOI: 10.1007/s00723-011-0303-8.
(28) Blinc, R.; Mali, M.; Osredkar, R.; Prelesnik, A.; Seliger, J.; Zupancic, I.; Ehrenberg, L. *J. Chem. Phys.* **1972**, *57*, 5087−5093.
(29) Edmonds, D. T. *Phys. Rep.* **1977**, *29*, 234−290.
(30) Seliger, J.; Žagar, V. *J. Magn. Reson.* **2008**, *193*, 54−62.
(31) Seliger, J.; Žagar, V.; Blinc, R. *J. Magn. Reson. A* **1994**, *106*, 214−222.
(32) Seliger, J.; Žagar, V.; Blinc, R. *Z. Naturforsch. A* **1994**, *49*, 31−34.
(33) Frisch, M. J.; Trucks, G. W.; Schlegel, H. B.; Scuseria, G. E.; Robb, M. A.; Cheeseman, J. R.; Montgomery, J. A. Jr.; Vreven, T.; Kudin, K. N.; Burant, J. C.; Millam, J. M.; Iyengar, S. S.; Tomasi, J.; Barone, V.; Mennucci, B.; Cossi, M.; Scalmani, G.; Rega, N.; Petersson, G. A.; Nakatsuji, H.; Hada, M.; Ehara, M.; Toyota, K.; Fukuda, R.; Hasegawa, J.; Ishida, M.; Nakajima, T.; Honda, Y.; Kitao, O.; Nakai, H.; Klene, M.; Li, X.; Knox, J. E.; Hratchian, H. P.; Cross, J. B.; Bakken, V.; Adamo, C.; Jaramillo, J.; Gomperts, R.; Stratmann, R. E.; Yazyev, O.; Austin, A. J., Cammi, R.; Pomelli, C.; Ochterski, J. W.; Ayala, P. Y.; Morokuma, K.; Voth, G. A.; Salvador, P.; Dannenberg, J. J.; Zakrzewski, V. G.; Dapprich, S.; Daniels, A. D.; Strain, M. C.; Farkas, O.; Malick, D. K.; Rabuck, A. D.; Raghavachari, K.; Foresman, J. B.; Ortiz, J. V.; Cui, Q.; Baboul, A. G.; Clifford, S.; Cioslowski, J.; Stefanov, B. B.; Liu, G.; Liashenko, A.; Piskorz, P.; Komaromi, I.; Martin, R. L.; Fox, D. J.; Keith, T.; Al-Laham, M. A.; Peng, C. Y.; Nanayakkara, A.; Challacombe, M.; Gill, P. M. W.; Johnson, B.; Chen, W.; Wong, M. W.; Gonzalez, C.; Pople, J. A. *Gaussian 03*, revisionD. 01; Gaussian, Inc.: Wallingford CT, 2004.
(34) Becke, A. D. *J. Chem. Phys.* **1993**, *98*, 1372−1377.
(35) Lee, C.; Yang, W.; Parr, R. G. *Phys. Rev. B* **1988**, *37*, 785−789.
(36) Pyykko, P. *Mol. Phys.* **2008**, *106*, 1965−1974.
(37) Latosińska, J. N. *Int. J. Quantum Chem.* **2003**, *91*, 284−296.
(38) Bader, R. F. W. *Atoms in Molecules: A Quantum Theory*; Oxford University Press: Oxford, 1994.
(39) Espinosa, E.; Molins, E.; Lecomte, C. *Chem. Phys. Lett.* **1998**, *285*, 170−173.
(40) Maruizumi, T.; Hiyama, Y.; Watanabe, N.; Niki, E. *Bull. Chem. Soc. Jpn.* **1978**, *51*, 978−980.
(41) Blinc, R.; Mali, M.; Osredkar, R.; Prelesnik, A.; Seliger, J.; Zupancic, I.; Ehrenberg, L. *J. Chem. Phys.* **1972**, *57*, 5087−5093.
(42) Maruizumi, T.; Hiyama, Y; Niki, E *Nippon Kagaku Kaishi* **1980**, *6*, 787−791.
(43) Singh, P.; Hodgson, D. J. *Acta Crystallogr. B* **1974**, *30*, 1430−1435.
(44) Ferrari, M. B.; Fava, G. G.; Pelosi, G.; Rodriguez-Arguelles, M. C.; Tarasconi, P. *J. Chem. Soc., Dalton Trans.* **1995**, 3035−3040.
(45) Stewart, R. F.; Jensen, L. H. *Acta Crystallogr.* **1967**, *23*, 1102−1105.
(46) Portalone, G.; Bencivenni, L.; Colapietro, M.; Pieretti, A.; Ramond, F. *Acta Chem. Scand.* **1999**, *53*, 57−68.
(47) Munshi, P.; Row, T. N. G. *Acta Crystallogr. B* **2006**, *62*, 612−626.
(48) Shefter, E.; Mautner, H. G. *J. Am. Chem. Soc.* **1967**, *89*, 1249−1253.
(49) Delage, C.; H'Naifi, A.; Goursolle, G.; Carpy, A. *C. R. Acad. Sci. Paris* **1986**, *302-II*, 219−222.
(50) Koch, P. L. A.; Popelier, A. *J. Phys. Chem.* **1995**, *99*, 9747−9754.
(51) Jeffrey, G. A. An Introduction to Hydrogen Bonding. In *Topics in Physical Chemistry*; Truhlar, D. G. Ed.; Oxford University Press: New York, 1997; p 303.
(52) See for example: Seliger, J. *Acta. Chim. Slov.* **2011**, *58*, 471−477 and the references cited therein.
(53) Schempp, E.; Bray, P. J. *J. Chem. Phys.* **1967**, *46*, 1186−1190.
(54) Rubenacker, G. V.; Brown, T. L. *Inorg. Chem.* **1980**, *19*, 392−398.
(55) Seliger, J.; Žagar, V. *J. Phys. Chem. A* **2010**, *114*, 12083−12087.